ORIGINAL ARTICLE

Journal Section

Influence of submeso motions on scalar oscillations and surface energy balance

Michel Stefanello[1] | Daniela Cava[2] | Umberto Giostra[3] | Otávio Acevedo[1] | Gervasio Degrazia[1] | Domenico Anfossi[4] | Luca Mortarini[1,4]

[1]Universidade Federal de Santa Maria, Santa Maria, Brazil

[2]Institute of Atmospheric Sciences and Climate - National Research Council, Lecce, Italy

[3]Department of Pure and Applied Sciences (DiSPeA), Università degli Studi di Urbino "Carlo Bo", Urbino, Italy

[4]Institute of Atmospheric Sciences and Climate - National Research Council, Turin, Italy

Correspondence
Daniela Cava, Institute of Atmospheric Sciences and Climate - National Research Council, Lecce, Italy
Email: d.cava@isac.cnr.it

Funding information
This study was financed in part by the Coordenação de Aperfeiçoamento de Pessoal de Nível Superior - Brasil (CAPES) - Finance Code 001 and by Programa de Doutorado Sanduíche no Exterior (PDSE)-CAPES under Process no. 88881.189395/2018-01

The presence of wave-like structures in the planetary boundary layer and their influence on the scalar fluxes and on the surface energy balance were investigated analyzing one year of continuous measurements collected in southern Brazil. Submeso oscillating patterns in the wind velocity components, temperature and scalar (CO_2, H_2O) concentrations were isolated using their auto-correlation functions. The analysis showed that low-wind speeds are necessary to trigger wavy motions. During nighttime, in presence of large vertical temperature gradient, horizontal meandering and internal gravity waves are dominant features of the stable boundary layer. Furthermore, a significant number of meandering cases was identified also during daytime in neutral conditions associated ~~to~~ with low values of net radiation. One case study showed how, during daytime, the wave-like patterns may be triggered by variations in the net radiation. Spectral analysis on the whole dataset showed that oscillations in the wind velocity and temperature field are frequently associated with CO_2 and H_2O wavy patterns with similar timescales. These non-turbulent oscillations produce unpredictable large scale contributions to vertical fluxes of temperature and scalar concentrations. The energy budget analysis showed how the choice of a proper averaging

time filters out these contributions and improves the energy budget closure, as well as the estimation of the net ecosystem exchange. The results confirm the influence of submeso motions in scalar dispersion, flux patterns and surface energy balance during low wind speed conditions and stable stratification.

KEYWORDS
Horizontal Meandering 1, Turbulent Fluxes 2, Surface Energy Balance 3, Low-wind conditions,4, Internal Gravity Waves 5, wave-turbulence interaction 6, very stable boundary layer 7

1 | INTRODUCTION

The Planetary Boundary Layer (PBL) is strongly influenced by the radiative diurnal cycle that drives the vertical thermal stratification. In unstable conditions (often dominated by weak horizontal winds) the turbulence production is mainly enhanced by buoyancy. On the other hand, in stable conditions the turbulent heat flux induced by the thermal stratification weakens the mechanical production of turbulence associated with the wind shear.

Scenarios of low-wind conditions are often associated with weak, intermittent and non-stationary turbulent patterns, often superimposed to a complex mix of larger scale processes that are generally difficult to measure and to parameterize. These processes are called submeso motions (Mahrt, 2014) and are ubiquitous in the Stable Boundary Layer. They can simultaneously occur on a variety of scales between the main turbulent eddies (few meters) and the smallest mesoscale motions (few kilometers). Submeso motions may interact in a nonlinear way with turbulence, and may have a great influence on the turbulent kinetic energy and the turbulent fluxes, especially in stable conditions (Finnigan, 1999; Sun et al., 2002, 2015; Vickers and Mahrt, 2003, 2007). Submeso motions originate from a variety of physical mechanisms and may include different processes such as density currents, microfronts, gravity waves, horizontal meandering, etc, that may coexist as a complex stochastic mix in the PBL (Acevedo et al., 2014; Mahrt, 2009, 2014). In presence of low-wind speeds and strong stability, horizontal meandering and gravity waves may require particular attention (Cava et al., 2019a, 2017; Mortarini et al., 2019) for their possible interaction and their role in intermittent turbulent production.

In the atmosphere, vertical wave-like motions are one of the most common observed phenomena and play an important role in transporting momentum and energy (Nappo, 2002). In the SBL, waves are ubiquitous, however, they are rarely linear waves: they occur in local packets and consist of only a few cycles with changing amplitude and period. These non-stationary wavelike disturbances, often called "dirty" waves, frequently degrade and lead to the generation of intermittent turbulence influencing turbulent transport of momentum, mass and energy in the SBL (Cava et al., 2015; Durden et al., 2013; Mahrt, 2014).

Horizontal meandering is another category of wave-like submeso motions that characterize the structure of the very stable boundary layer (Mortarini et al., 2019). Horizontal meandering manifests itself as large non-turbulent oscillations of the horizontal wind velocity components and temperature, associated ~~to~~ with a peak in the low-frequency range of the correspondent spectra (Mortarini et al., 2016a,b). It was often observed near the surface in low-wind conditions, but it was recently identified at higher heights and wind speeds (Mortarini et al., 2019). Since meandering motions are generally related to large variations of the wind direction they may significantly influence the ~~pollutant~~

scalar horizontal dispersion in particular in low-wind speed and in very stable conditions or, in general, in presence of a weak vertical turbulent mixing (Anfossi et al., 2006; Mahrt and Mills, 2009; Mortarini et al., 2019). Though meandering modes are more common in stable atmospheric stratification at night-time, they were also observed during daytime in calm conditions (Anfossi et al., 2005; Mortarini et al., 2016b; Oettl et al., 2005; Vickers et al., 2008). Nonetheless, the physical causes responsible for horizontal meandering are not yet well understood in both stable and unstable atmospheric stratifications. Possible sources may be orographic features, horizontal temperature gradients, pulsating drainage flows or surface pressure perturbations induced by mesoscale motions (Mahrt, 2014).

Recent studies have made advances in describing the interplay between turbulence and submeso motions (Cava et al., 2019a,b, 2017; Kang et al., 2015; Mortarini et al., 2018, 2016a,b; Vercauteren and Klein, 2015; Vercauteren et al., 2016). However, a good understanding of their complex interaction remains a challenging task for a correct estimation of the land-surface exchange, for a correct parameterization of the turbulent fluxes and for the improvement of numerical model performance, in particular in low-wind speed conditions. In fact, due to a still incomplete knowledge of their dynamics and physics causes, submeso motions are not generally represented in numerical models (Belušić and Güttler, 2010).

The goal of this study is to investigate the impact of submeso motions on scalar oscillations and on the closure of the surface energy balance during the daily cycle.

In any ecosystem, the energy balance between the land surface and the atmosphere is one of the fundamental processes. How the turbulent sensible and latent heat fluxes are partitioned at the surface plays a crucial role in determining the boundary layer development, the hydrological cycle, as well as weather and climate evolution (Falge et al., 2005). The understanding of the factors that mainly affect the closure of the surface energy balance remains an unsolved problem in micrometeorology and has strong implications on the interpretation of the energy flux measurements and on their comparison to model simulations (Foken, 2008; Foken et al., 2011; Leuning et al., 2012; Oncley et al., 2007). In literature an average budget imbalance between 10% and 30% was found and different reasons were proposed to explain it (errors in measurements of each component of the energy balance, mismatch in the instrument footprints, vertical divergence of the flux, advection, inadequate sampling of large scale eddies, complex surface heterogeneity, passage of clouds). The global energy budget may be improved applying different correction terms that cancel energy residuals of opposite sign. However, such residuals usually remain not negligible both during daytime and during the night (Cava et al., 2008). In particular, different processes typical of low-wind nocturnal conditions (i.e. low level of turbulence, intermittency, submeso motions, dew formation) may have a large impact on the energy balance closure. Large imbalance is reported when the vertical fluxes are too weak to balance the radiative cooling at the surface (Van de Wiel et al., 2017). Under these conditions the eddy-covariance method may underestimate the true atmospheric exchange. A threshold on the friction velocity (< 0.2 m s^{-1}) is frequently used to discard data associated ~~to~~ with poorly developed turbulence (Barr et al., 2013; Cui and Chui, 2019; Goulden et al., 1996; Reichstein et al., 2005). However, to reduce the number of discarded data, a proper averaging time (instead of the standard 30-minutes averaging time) that takes into account the influence of submeso activity on the turbulent fluxes (Vickers and Mahrt, 2006) may provide a proper estimation of the turbulent fluxes and, consequently, improve the closure of the energy balance. For investigating the submeso motions impact on the surface energy balance and on the oscillation of scalars (temperature, water vapour and CO_2 concentration), one year of data collected at south Brazil were analyzed. The identification of submeso events and their characteristic time-scales was carried out by means of Eulerian autocorrelation functions and spectral analysis of the wind velocity components and temperature (Anfossi et al., 2005; Mortarini et al., 2016a,b).

2 | EXPERIMENTAL SITE

The dataset used in the present study was obtained at the Federal University of Santa Maria (Rio Grande do Sul, Brazil) experimental site (Roberti et al., 2012). The site is located in a pampa biome area of 24 ha of natural pasture, characterized by extensive and flat treeless grassland area with a shallow sandy-loam soil (Rubert et al., 2018). The data was collected from December 2015 to November 2016 on a 30 m high micrometeorological tower installed at $29°43'27.502''S$; $53°45'36.097''W$; 88 m ~~elevation~~ amsl (above mean sea level). Measurements of wind velocity components (u, v, w) and sonic temperature (T) were sampled at a frequency of 10 Hz by sonic anemometer installed at 3 m (from December 2015 to 15 June 2016; Wind Master Pro-Gill Instruments and after by IRGASON-Campbell Scientific) and 30 m (CSAT3-Campbell Scientific), while measurement of H_2O and CO_2 concentration were sampled at a frequency of 10 Hz at 3 m (from December 2015 to 15 June 2016 by a gas analyzer LI7500-LI-COR and after 15 June 2016 by a IRGASON-Campbell Scientific).

Standard meteorological variables as air temperature, T_{air}, and relative humidity, RH, were collected by three slow response thermo-hygrometers (HMP155-Vaisala) located above the ground at the heights of 3, 9 and 30 m and sampled each 5 seconds from December 2015 to June 2016 and after this period each minute. Additional sensors were installed to measure the surface energy balance. Net radiation, Rn, and short-wave incident radiation were sampled each minute by CNR4-Kipp & Zonen sensors located at 3 m above the ground. The soil heat flux, G_m, was measured by Thermal Sensors (HFP01-Hukseflux) located at 0.10 m depth, while the soil temperature, T_s, was measured by temperature probes (T108-Campbell Scientific) at three depths (0.05, 0.10 and 0.30 m). Soil variables were sampled each 2 minute from December 2015 to June 2016 and after this period were measured each minute. Due to technical problems, data from 16 June 2016 to 02 September 2016 were not considered in the present study.

3 | IDENTIFICATION OF MEANDERING AND GRAVITY WAVES.

To study the influence of submeso structures on scalar oscillations and their impact on the surface energy balance data were first divided ~~in~~ into subset of one hour and then rotated in a streamline coordinate system, applying a double rotation (Cassardo et al., 1995; McMillen, 1988). The larger submeso motions, represented mainly by the horizontal wind meandering, may have characteristics time scales that rarely exceeds 40 minutes, thus, the choice of a 1-hour averaging window seems appropriate. Since one of the main purposes of this paper is to investigate the influence of wave-like oscillations on the scalar flux behaviour, the 1-hour data subsets were divided ~~in~~ into meandering and non-meandering cases applying the Eulerian autocorrelation function (EAF) analysis described in Mortarini et al. (2016a) and Cava et al. (2019b). In presence of meandering the EAFs frequently exhibit an oscillatory behaviour that can be described by the following equation:

$$R_c(\tau) = \frac{\langle c(t+\tau)c(t)\rangle}{\sigma_c^2} = e^{-p_c\tau}cos(q_c\tau) \quad \text{with } c = u, v, w, T, \tag{1}$$

where τ is the temporal lag and σ_c^2 is the variance of the variable c. The p parameter is connected to the turbulence de-correlation time scale, while the parameter q defines the meandering period:

$$T_* = \frac{2\pi}{q}. \tag{2}$$

The ratio between q and p represents the looping parameter m:

$$m = \frac{q}{p}. \tag{3}$$

Values of $m < 1$ indicate that the turbulent exponential decay prevails on the oscillating part of the EAF, whereas values of $m > 1$ indicate a boundary layer dynamics in which non-turbulent wave-like motions play an important role. Mortarini et al. (2016a,b) classified as "meandering" episodes the hours when m_u, m_v and m_T are simultaneously larger than 1 and as "non-meandering" episodes the hours when the theoretical formulation (Eq.1) is not able to fit the observed EAF (for a detailed description of the fitting method, see Cava et al. (2019a)). A previous study (Mortarini et al., 2019) pointed out that mixed cases (where just one or two components oscillate or where Eq. 1 fits the data but with $m < 1$) show an intermediate behaviour between meandering and non-meandering cases, probably due to an intrinsic difficulty in separating the flow dynamics in just two non-overlapping behaviours.

In the present study the data clusterization in wave-like (meandering, m_u, m_v, $m_T > 1$) and non-wave-like behaviours (non-meandering, Eq. 1 does not represent the measured EAF for u,v and T) was performed on the basis of the results of the EAF technique applied to data collected at the highest level. Then, the behaviour of the flow variables in the 916 meandering cases detected at 30m was checked also at the lowest level: at 3 m about 55% of the these data were classified as "meandering" in the sense of (Mortarini et al., 2019), $\sim$ 43% were classified as "mixed cases" and only $\sim$ 2% were classified as "non-meandering". The comparison of the results obtained at the two levels suggests that meandering is not a local phenomenon, as previously observed elsewhere (Mortarini et al., 2018, 2019). However, in order to guarantee the vertical coherence of meandering and remove ambiguous cases, the $\sim$ 2% of "non-meandering" hours detected at 3 m was excluded in the analysis. As a result, in the final selection 900 hours were classified as "meandering cases" and 1717 hours were classified as "non-meandering cases". Table 1 shows the number of meandering and non-meandering occurrences for the analyzed experiment in the different hours of the day. Noteworthy, meandering cases were mainly observed during the night and in the transition periods (around sunrise and sunset). During nighttime buoyancy acts to destroy turbulence and submeso motions may dominate the flow dynamics, in particular in low wind conditions. On the other hand, few cases were detected during daytime when the turbulent convection may inhibit submeso oscillations. "Non-meandering" cases are quite evenly distributed during the daily cycle because usually associated ~~to~~ with mechanical production of turbulence.

As shown by Cava et al. (2017), the EAF fitting procedure can be extended beyond the identification of waves in the horizontal wind velocity field. In section 4.2 the EAF of the vertical component of the wind velocity is fitted against Eq.(1) to detect the presence of internal gravity waves. Further, the EAFs of the concentration of CO_2 and of H_2O were evaluated to study the influence of wave-like motions on the scalars behaviour.

4 | DATA ANALYSIS

~~For studying~~ To study the impact of submeso motions on the surface energy balance and on the scalar oscillations, only the data at the lowest level were taken into account. This choice was motivated by the availability of the latent heat flux measurements exclusively at 3m and to reduce errors associated with the vertical flux divergence in the stable boundary layer (Mahrt et al., 2018).

Figure 1 shows the boxplot of the mean net radiation (Rn), vertical air temperature difference (ΔT_{air}) between 30 and 3 m and the mean wind speed measured at 3 m for meandering and non-meandering cases. All the quantities are evaluated averaging over 1-hour. Horizontal modes occurred during the night in low-wind conditions and in presence

of a large vertical air temperature difference (ΔT_{air}), indicative of a strong stratification in the stable boundary layer. No clear difference was observed between meandering and non-meandering cases in the nocturnal Rn values. On the other hand, horizontal meandering was observed during daytime in presence of a low positive radiative forcing, often related to cloudy conditions, weak synoptic flows and weak vertical air temperature gradient (ΔT_{air}) associated ~~to~~ with an almost neutral atmosphere. In the following we will refer to large scales as temporal and spacial length scales that are larger than the typical turbulent scales.

In section 4.1 a ~~diurnal~~ daytime meandering episode was selected as a case study to investigate the characteristics of horizontal oscillations during ~~diurnal~~ daytime conditions. In section 4.2 the features of observed nocturnal submeso motions and their impact on scalar transport were discussed. Finally, in section 4.3 the influence of submeso oscillations on the surface energy balance was explored.

4.1 | Daytime horizontal meandering

As already discussed in the previous section, ~~diurnal~~ daytime horizontal meandering was observed in the analyzed data-set in conditions of low Rn values, indicative of cloudy conditions. Figure 2 shows an example of a ~~diurnal~~ daytime period characterized by the presence of horizontal meandering measured on 21 December 2015 between 1200 and 1600 LST (local standard time). Even if the mean wind speed at 3 m in the first hour was 3 m s^{-1}, the successive hours were characterized by low wind speed values (ranging from 0.6 m s^{-1} to 1.7 m s^{-1} at the lowest level), whereas for the entire period the net radiation ranged from 19 W m^{-2} to 125 W m^{-2}. The observed micro-meteorological parameters indicated an almost neutral boundary layer, characterized by low speed and weak vertical turbulent mixing. As a matter of fact, the period was characterized by the stability parameter $z/L = 0.005 \pm 0.020$, being z the height of measurements (3 m) and L the Obukhov length.

The horizontal wind velocity components show an oscillatory behaviour at both levels (Fig. 2a,b), more evident between 1330 and 1545 LST. Similar oscillations are clearly detected in the air temperature time series (Fig. 2d) and they are less markedly observed in the net radiation signal (Fig. 2e), likely modulated by the passage of clouds. The vertical velocity component is characterized by high frequency fluctuations and does not exhibit the oscillatory behaviour observed in the other variables. (Fig. 2c).

The oscillatory behaviour of the time series was investigated by means of the EAFs and spectral analysis. Fig. 3 features the EAFs (a) and spectra (b) of the horizontal wind velocity components collected at the lowest level between 1400 to 1600 LST of 21 December 2015. Fig. 4 shows the correspondent quantities for the vertical velocity component, the sonic temperature and the net radiation. A clear negative lobe, distinctive of the oscillatory behaviour, can be observed in the EAFs of all the depicted quantities but the vertical wind velocity component. Note the good agreement of experimental and theoretical behaviour of EAFs (Anfossi et al., 2005), as well as of experimental spectra and the spectral model in low wind conditions proposed by (Mortarini et al., 2016a). The spectra of horizontal components, sonic temperature and Rn exhibit a low-frequency peak associated ~~to~~ with the energy of submeso contribution. The spectrum of the vertical velocity component presents the typical behaviour of a turbulence spectrum, in agreement with the quick decay of its EAF. Table 2 shows the meandering time-scales evaluated fitting the experimental EAFs with Eq. 1 and then using Eq. 2. Noteworthy, the different variables exhibit similar T_*, coincident with the time scales associated ~~to~~ with the low-frequency energetic peaks in their spectra (Figs. 3b and 4b). The presence of the low-frequency spectral peak in the Rn spectrum confirms a possible correlation of observed ~~diurnal~~ daytime meandering and Rn behaviour.

4.2 | Submeso motions and their impact on the nocturnal scalar transport

The largest part of the detected meandering cases occurred during nighttime, as reported in Table 1 (676 cases, i.e. 75% of the 900 total cases). Figure 5 shows the boxplots of the time scales (Eq. 2) for the wind velocity components (u, v, w) and the scalars (T, CO_2, H_2O) relative to the nocturnal meandering cases. The medians of the meandering time scales for all the analyzed variables ranged between 1600 s and 1800 s. Noteworthy, a large percentage of nocturnal meandering cases was associated ~~to~~ with CO_2 and H_2O oscillations (70% and 84%, respectively); moreover, about 25% of them was also associated ~~to~~ with wave-like behaviour in the vertical velocity component during the night. The observed large percentage of scalar oscillations, whose time scales are comparable to those of the horizontal velocity components, highlights the important role of meandering in influencing the horizontal dispersion of scalars (Anfossi et al., 2006).

Figure 6 displays the averaged normalized spectra of wind velocity components (a,b) and of scalars (c,d) relative to the nocturnal meandering cases. The single spectra were calculated for a time window of 1 h and then the ensemble averages were computed. As previously observed, about 25% of the nocturnal horizontal meandering cases are also characterized by clear vertical oscillations ($m_w > 1$); therefore the spectra are separately averaged considering cases with the coexistence of horizontal and vertical submeso motions (right column in Figure 6) or exclusively considering horizontal meandering (left column in Figure 6). All the normalized averaged spectra follow the Kolmogorov (1941) theory in the high-frequency range. On the other hand, the spectra of the horizontal velocity components and the scalars deviate from the standard turbulent spectra behaviour at low frequencies exhibiting a marked secondary peak. Such large scale spectral energy is clearly evident also in the vertical spectrum in presence of simultaneous horizontal and vertical submeso oscillations (Fig. 6b). The spectral peaks at low frequency for the wind velocity components and the scalars are coincident and in a good agreement with the ranges of time scales estimated by the EAF technique (see Figure 5).

Figure 7 shows the averaged normalized co-spectra for wT, wH_2O and wCO_2, in the presence (b) and absence (a) of submeso motions. As well as for the averaged spectra, single co-spectra were computed for a time window of 1 h, normalized with the absolute value of the correspondent kinematic flux, and then averaged over all detected cases. Co-spectra relative to non-meandering cases (Figure 7a) exhibit the typical behaviour of turbulent co-spectra with a main peak located at around 10 s ($f \sim 0.1$ Hz) for all the three scalar fluxes. All the averaged co-spectral intensities decrease at larger scales and assume negligible values at a time scale of about 10 min ($f \sim 0.0016$ Hz). On the other hand, the effect of submeso motions on scalar fluxes is more complex and may produce large errors in sign and magnitude of the computed fluxes. In fact, averaged co-spectra relative to meandering cases (Fig. 7b) present the small-scale turbulent peak at around 10 s ($f \sim 0.1$ Hz); then their intensities significantly decrease at a time scale of about 2 min ($f \sim 0.008$ Hz), but exhibit a random behaviour at larger scales. If not correctly filtered, these extremely large co-spectral values and ~~unrealistic~~ random bursts associated ~~to~~ with submeso motions may lead to misinterpretations of the turbulent fluxes.

Comparing the turbulent portions of the co-spectra for the two different flow dynamics, it is possible to observe that for meandering cases wH_2O co-spectra can assume both positive and negative values. While positive values correspond to evaporation, negative values of wH_2O are related to downward flux of water vapour associated ~~to~~ with dew formation, favoured during low wind speeds, stably stratified conditions and moist atmosphere (de Roode et al., 2010). Figure 8 displays the boxplots of the relative humidity (RH) as a function of the daily cycle for meandering and non-meandering cases. The values of RH close to saturation (100 %) in meandering cases during the night confirm that low-wind speed conditions are often associated with dew deposition, as observed in Price (2019); Ritter et al. (2019); de Roode et al. (2010).

On the basis of the observed co-spectral behaviour, different averaging times were chosen for the computation of

the turbulent fluxes for non meandering cases (T_{ave}=10 min) and for meandering cases (T_{ave}=2 min), in order to filter out the submeso contributions and to correctly estimate the turbulent transport.

In the next section the implications of the choice of the different averaging time in the estimation of the surface energy balance will be discussed.

4.3 | Surface Energy balance

Figure 9 shows the boxplot of diurnal variation of soil heat flux (G), sensible heat flux (H) and latent heat flux (LE) under meandering (orange) and non-meandering (blue) conditions. The soil heat flux (G) was evaluated for each hour as (Cava et al., 2008):

$$G = G_m + S \tag{4}$$

where G_m is the measured soil heat flux averaged over one hour and $S = c_v \Delta z \, (\Delta T_s / \Delta t)$ is the soil storage, where c_v=1.3x10^6 Jm^{-3}K^{-1} is the soil volumetric heat capacity, Δz is the depth of the plate below the ground, $\Delta T_s / \Delta t$ is soil temperature gradient over the hour.

Turbulent scalar flux of water vapor and carbon dioxide was corrected for the effects of density following Webb et al. (1980) to account density effect due to both thermal expansion and water vapor dilution of the air. The turbulent fluxes, H and LE, were evaluated during the nighttime using the averaging time of 10 min and 2 min for non-meandering and meandering cases, respectively. The averaging time were chosen following the co-spectral analysis results (section 4.2). On the basis of a similar analysis performed on ~~diurnal~~ daytime hours (not shown), 1 hour and 15 minutes have been used, respectively, as averaging time for non-meandering and meandering cases during daytime. In presence of meandering, turbulent fluxes H and LE assume low values both in ~~diurnal~~ daytime and ~~nocturnal~~ nighttime hours. Differently, soil heat flux tends to assume larger values (in magnitude) when compared to non-meandering cases. In particular, during nighttime turbulent fluxes assume values very close to zero and represent a small fraction of the surface energy budget. In these conditions, generally associated ~~to~~ with a very strong atmospheric stratification and low wind conditions (cf. Figure 1) the soil heat flux plays a major role in balancing the radiative loss at the surface. During daytime, the low values of turbulent fluxes in meandering cases are associated with weak convection in cloudy conditions as shown in Fig. 1, while no clear differences were observed in the soil heat flux values between meandering and non-meandering cases.

Figure 10 shows the inter-comparison between the turbulent heat fluxes ($H + LE$) and the available energy ($Rn - G$). In these plots, orange dots represent meandering cases and blue dots represents non-meandering cases. In Figure 10a the turbulent fluxes were computed using the "standard" one hour averaging time, while in Figure 10b the appropriate period of time derived from the co-spectra analysis was used. The global closure rate of the surface energy balance, derived from the slope of the linear fit of ($H + LE$) vs. ($Rn - G$), is $\approx$ 79%. The observed imbalance is in agreement with typical values obtained in the same site (Rubert et al., 2018) or in other experiments (Majozi et al., 2017; Soltani et al., 2017). It is noteworthy that, although the global rate does not change by applying different averaging periods, the use of a correct averaging time produces an improvement of the coefficients of determination (R^2) (from 0.76 to 0.90) and, in particular, an evident reduction in the spread of the data associated ~~to~~ with the meandering cases. The importance of a proper choice of the averaging time for calculating the turbulent statistics is confirmed by the attenuation of energy residual during nighttime (Fig.11). The decrease of energy residual is particularly evident for meandering cases (Figure 11c), associated ~~to~~ with very stable and low-wind conditions, as highlighted by the number of cases associated ~~to~~ with

the different classes of wind speed.

To further investigate the influence of the submeso motions on the scalar transport, the CO_2 vertical fluxes were computed using different averaging periods (Figure 12). Whereas the choice of a different averaging time slightly affects the CO_2 vertical fluxes during non-meandering hours, large differences are observed during periods associated ~~to~~ with horizontal meandering, in particular in very low-speed conditions. The result confirms the importance of the choice of the averaging period to minimize the "contamination" of the CO_2 vertical fluxes, as well as other turbulent fluxes, by submeso-motions that, if not filtered, may produce ~~non-physical~~ erratic values of turbulent statistics (as negative CO_2 vertical fluxes associated ~~to~~ with nocturnal CO_2 respiration).

Finally, it should be noted that the meandering cases represent an important fraction of the entire nocturnal data-set (27%) and that they are usually associated with very stable conditions, therefore with low-values of friction velocity u_* (Fig. 13). Typically, u_* values of the order of 0.2 m s^{-1} were used as a threshold to filter data in the surface energy balance as well in the estimation of net ecosystem exchange (Cui and Chui, 2019; Reichstein et al., 2005). The obtained results show that the proper choice of the averaging time may reduce the number of discarded time series, improving the statistical significance of both surface energy balance and flux budget.

5 | CONCLUSIONS

The main goal of this study was to investigate the influence of horizontal meandering on scalar oscillations and on the surface energy balance. The analysis was performed using one year of data collected at the experimental site of the Federal University of Santa Maria located in southern Brazil. The Eulerian autocorrelation function technique and the spectral analysis were employed to detect "meandering" and "non-meandering" hours and to study their characteristics. Horizontal meandering was defined as simultaneous oscillations of horizontal wind components and temperature. It was frequently observed during nighttime in presence of low-wind and strong radiative cooling conditions typical of strong stratification of the boundary layer. Noteworthy, a moderate amount of cases was also observed during daytime associated with low radiative forcing, cloudy conditions and weak synoptic flows. One case study showed that the ~~diurnal~~ daytime wave-like patterns may be triggered by variations in the net radiation. A representative ~~diurnal~~ daytime case study of wave-like patterns indicated that oscillations in the horizontal components and temperature may be generated by variations in the net radiation. During nighttime vertical waves coexisted with horizontal oscillations in about 25% of cases with comparable time scales. Moreover, a large percentage of horizontal meandering cases appeared associated with CO_2 and H_2O oscillations (about 70% and 84%, respectively) characterized by time scales similar to those observed for the wind velocity components and temperature ($T_* \simeq$ 1600 to 1800 s).

Co-spectral analysis highlighted the role of submeso oscillations in producing random and unpredictable low-frequency contributions to vertical fluxes of temperature and scalar concentrations. The high variability in magnitude and sign of submeso fluxes is because they are not driven by local gradients. Further, during very stable conditions, such motions may be very poorly sampled and, therefore, their inclusion might increase the flux uncertainty and should be filtered for a proper estimation of surface energy balance.

Nocturnal co-spectra relative to non-meandering cases exhibit the typical behaviour of turbulent co-spectra, assuming negligible values at a time scale of about 10 min. On the other hand, the nocturnal meandering co-spectra present a peak related to the small turbulent scales (at around 10 s) and random contributions at scales larger than 2 min that may produce large errors in sign and magnitude of the computed fluxes. Therefore, in order to filter out such submeso contributions, different averaging times were chosen for the computation of the nocturnal turbulent fluxes for non-meandering cases (10 min) and for meandering cases (2 min). On the basis of the cospectral analysis performed

on ~~diurnal~~ daytime hours, 1 hour and 15 minutes were used, respectively, as averaging time for non-meandering and meandering cases during daytime.

The application of the proper averaging time in the different cases, instead of the standard time (1 hour), improved the estimation of the surface energy balance producing the reduction in the spread of the data associated ~~to~~ with the meandering cases and an evident attenuation of nocturnal energy residual associated ~~to~~ with very stable and low-wind conditions. Furthermore, the use of different averaging times allowed the minimization of the contamination of vertical CO_2 fluxes by submeso motion that, if not filtered, may produce ~~non-physical~~ erratic fluxes (as negative CO_2 vertical fluxes associated ~~to~~ with nocturnal CO_2 respiration). Typically these ~~unrealistic~~ erratic values are associated ~~to~~ with low values of friction velocities and are discarded from the analysis by using a threshold value of u_*. The obtained results show that, as the meandering cases represent an important fraction of the entire nocturnal data-set, the proper choice of the averaging time may reduce the number of discarded time series, improving the statistical significance of the estimation of both surface energy balance and net ecosystem exchange.

The results obtained in this study confirmed the importance of the submeso motions in influencing the characteristics of the atmospheric flow in low-wind conditions and in particular in the very stable boundary layer.

ACKNOWLEDGEMENTS

The Santa Maria site has been deployed and maintained by the Laboratório de Micrometeorologia of the Universidade Federal de Santa Maria, lead by Prof. Debora R. Roberti. This study was financed in part by the Coordenação de Aperfeiçoamento de Pessoal de Nível Superior - Brasil (CAPES) - Finance Code 001 and by the Programa de Doutorado Sanduíche no Exterior (PDSE)-CAPES under Process no. 88881.189395/2018-01.

REFERENCES

Acevedo, O. C., Costa, F. D., Oliveira, P. E., Puhales, F. S., Degrazia, G. A. and Roberti, D. R. (2014) The influence of submeso processes on stable boundary layer similarity relationships. *Journal of the Atmospheric Sciences*, **71**, 207–225.

Anfossi, D., Alessandrini, S., Castelli, S. T., Ferrero, E., Oettl, D. and Degrazia, G. (2006) Tracer dispersion simulation in low wind speed conditions with a new 2d langevin equation system. *Atmospheric Environment*, **40**, 7234–7245.

Anfossi, D., Oettl, D., Degrazia, G. and Goulart, I. (2005) An analysis of sonic anemometer observations in low wind speed conditions. *Boundary-Layer Meteorology*, **114**, 179–203.

Barr, A., Richardson, A., Hollinger, D., Papale, D., Arain, M., Black, T., Bohrer, G., Dragoni, D., Fischer, M., Gu, L. et al. (2013) Use of change-point detection for friction–velocity threshold evaluation in eddy-covariance studies. *Agricultural and Forest Meteorology*, **171**, 31–45.

Belušić, D. and Güttler, I. (2010) Can mesoscale models reproduce meandering motions? *Quarterly Journal of the Royal Meteorological Society: A journal of the atmospheric sciences, applied meteorology and physical oceanography*, **136**, 553–565.

Cassardo, C., Sacchetti, D., Morselli, M., Anfossi, D., Brusasca, G. and Longhetto, A. (1995) A study of the assessment of air temperature, and sensible-and latent-heat fluxes from sonic-anemometer observations. *Il Nuovo Cimento C*, **18**, 419–440.

Cava, D., Contini, D., Donateo, A. and Martano, P. (2008) Analysis of short-term closure of the surface energy balance above short vegetation. *Agricultural and Forest Meteorology*, **148**, 82–93.

Cava, D., Giostra, U. and Katul, G. (2015) Characteristics of gravity waves over an antarctic ice sheet during an austral summer. *Atmosphere*, **6**, 1271–1289.

Cava, D., Mortarini, L., Anfossi, D. and Giostra, U. (2019a) Interaction of submeso motions in the antarctic stable boundary layer. *Boundary-Layer Meteorology*, 1–23.

Cava, D., Mortarini, L., Giostra, U., Acevedo, O. and Katul, G. (2019b) Submeso motions and intermittent turbulence across a nocturnal low-level jet: A self-organized criticality analogy. *Boundary-Layer Meteorology*, 1–27.

Cava, D., Mortarini, L., Giostra, U., Richiardone, R. and Anfossi, D. (2017) A wavelet analysis of low-wind-speed submeso motions in a nocturnal boundary layer. *Quarterly Journal of the Royal Meteorological Society*, **143**, 661–669.

Cui, W. and Chui, T. F. M. (2019) Temporal and spatial variations of energy balance closure across fluxnet research sites. *Agricultural and Forest Meteorology*, **271**, 12–21.

Durden, D., Nappo, C., Leclerc, M., Duarte, H., Zhang, G., Parker, M. and Kurzeja, R. (2013) On the impact of wave-like disturbances on turbulent fluxes and turbulence statistics in nighttime conditions: a case study. *Biogeosciences*, **10**, 8433–8443.

Falge, E., Reth, S., Brüggemann, N., Butterbach-Bahl, K., Goldberg, V., Oltchev, A., Schaaf, S., Spindler, G., Stiller, B., Queck, R. et al. (2005) Comparison of surface energy exchange models with eddy flux data in forest and grassland ecosystems of germany. *Ecological Modelling*, **188**, 174–216.

Finnigan, J. (1999) A note on wave-turbulence interaction and the possibility of scaling the very stable boundary layer. *Boundary-Layer Meteorology*, **90**, 529–539.

Foken, T. (2008) The energy balance closure problem: an overview. *Ecological Applications*, **18**, 1351–1367.

Foken, T., Aubinet, M., Finnigan, J. J., Leclerc, M. Y., Mauder, M. and Paw U, K. T. (2011) Results of a panel discussion about the energy balance closure correction for trace gases. *Bulletin of the American Meteorological Society*, **92**, ES13–ES18.

Goulden, M. L., Munger, J. W., Fan, S.-M., Daube, B. C. and Wofsy, S. C. (1996) Measurements of carbon sequestration by long-term eddy covariance: Methods and a critical evaluation of accuracy. *Global change biology*, **2**, 169–182.

Kang, Y., Belušić, D. and Smith-Miles, K. (2015) Classes of structures in the stable atmospheric boundary layer. *Quarterly Journal of the Royal Meteorological Society*, **141**, 2057–2069.

Kolmogorov, A. N. (1941) The local structure of turbulence in incompressible viscous fluid for very large reynolds numbers. In *Dokl. Akad. Nauk SSSR*, vol. 30, 301–305. JSTOR.

Leuning, R., Van Gorsel, E., Massman, W. J. and Isaac, P. R. (2012) Reflections on the surface energy imbalance problem. *Agricultural and Forest Meteorology*, **156**, 65–74.

Mahrt, L. (2009) Characteristics of submeso winds in the stable boundary layer. *Boundary-Layer Meteorology*, **130**, 1–14.

— (2014) Stably stratified atmospheric boundary layers. *Annual Review of Fluid Mechanics*, **46**, 23–45.

Mahrt, L. and Mills, R. (2009) Horizontal diffusion by submeso motions in the stable boundary layer. *Environmental Fluid Mechanics*, **9**, 443–456.

Mahrt, L., Thomas, C. K., Grachev, A. A. and Persson, P. O. G. (2018) Near-surface vertical flux divergence in the stable boundary layer. *Boundary-Layer Meteorology*, **169**, 373–393.

Majozi, N. P., Mannaerts, C. M., Ramoelo, A., Mathieu, R., Nickless, A. and Verhoef, W. (2017) Analysing surface energy balance closure and partitioning over a semi-arid savanna fluxnet site in skukuza, kruger national park, south africa. *Hydrology and Earth System Sciences*, **21**.

McMillen, R. T. (1988) An eddy correlation technique with extended applicability to non-simple terrain. *Boundary-Layer Meteorology*, **43**, 231–245.

Mortarini, L. and Anfossi, D. (2015) Proposal of an empirical velocity spectrum formula in low-wind speed conditions. *Quarterly Journal of the Royal Meteorological Society*, **141**, 85–97.

Mortarini, L., Cava, D., Giostra, U., Acevedo, O., Nogueira Martins, L., Soares de Oliveira, P. and Anfossi, D. (2018) Observations of submeso motions and intermittent turbulent mixing across a low level jet with a 132-m tower. *Quarterly Journal of the Royal Meteorological Society*, **144**, 172–183.

Mortarini, L., Cava, D., Giostra, U., Costa, F. D., Degrazia, G., Anfossi, D. and Acevedo, O. (2019) Horizontal meandering as a distinctive feature of the stable boundary layer. *Journal of the Atmospheric Sciences*, **76**, 3029–3046.

Mortarini, L., Maldaner, S., Moor, L., Stefanello, M., Acevedo, O., Degrazia, G. and Anfossi, D. (2016a) Temperature autocorrelation and spectra functions in low-wind meandering conditions. *Quarterly Journal of the Royal Meteorological Society*.

Mortarini, L., Stefanello, M., Degrazia, G., Roberti, D., Castelli, S. T. and Anfossi, D. (2016b) Characterization of wind meandering in low-wind-speed conditions. *Boundary-Layer Meteorology*, 1–18.

Nappo, C. J. (2002) *An introduction to atmospheric gravity waves*. Academic Press.

Oettl, D., Goulart, A., Degrazia, G. and Anfossi, D. (2005) A new hypothesis on meandering atmospheric flows in low wind speed conditions. *Atmospheric Environment*, **39**, 1739–1748.

Oncley, S. P., Foken, T., Vogt, R., Kohsiek, W., DeBruin, H., Bernhofer, C., Christen, A., Van Gorsel, E., Grantz, D., Feigenwinter, C. et al. (2007) The energy balance experiment ebex-2000. part i: overview and energy balance. *Boundary-Layer Meteorology*, **123**, 1–28.

Price, J. (2019) On the formation and development of radiation fog: An observational study. *Boundary-Layer Meteorology*, 1–31.

Reichstein, M., Falge, E., Baldocchi, D., Papale, D., Aubinet, M., Berbigier, P., Bernhofer, C., Buchmann, N., Gilmanov, T., Granier, A. et al. (2005) On the separation of net ecosystem exchange into assimilation and ecosystem respiration: review and improved algorithm. *Global Change Biology*, **11**, 1424–1439.

Ritter, F., Berkelhammer, M. and Beysens, D. (2019) Dew frequency across the us from a network of in situ radiometers. *Hydrology and Earth System Sciences*, **23**, 1179–1197.

Roberti, D. R., Acevedo, O. C. and Moraes, O. L. (2012) A brazilian network of carbon flux stations. *Eos, Transactions American Geophysical Union*, **93**, 203–203.

de Roode, S. R., Bosveld, F. C. and Kroon, P. S. (2010) Dew formation, eddy-correlation latent heat fluxes, and the surface energy imbalance at cabauw during stable conditions. *Boundary-Layer Meteorology*, **135**, 369–383.

Rubert, G., Roberti, D., Pereira, L., Quadros, F., Campos Velho, H. and Leal de Moraes, O. (2018) Evapotranspiration of the brazilian pampa biome: Seasonality and influential factors. *Water*, **10**, 1864.

Soltani, M., Mauder, M., Laux, P. and Kunstmann, H. (2017) Turbulent flux variability and energy balance closure in the tereno prealpine observatory: a hydrometeorological data analysis. *Theoretical and Applied Climatology*, 1–20.

Sun, J., Burns, S. P., Lenschow, D. H., Banta, R., Newsom, R., Coulter, R., Frasier, S., Ince, T., Nappo, C., Cuxart, J. et al. (2002) Intermittent turbulence associated with a density current passage in the stable boundary layer. *Boundary-Layer Meteorology*, **105**, 199–219.

Sun, J., Mahrt, L., Nappo, C. and Lenschow, D. H. (2015) Wind and temperature oscillations generated by wave–turbulence interactions in the stably stratified boundary layer. *Journal of the Atmospheric Sciences*, **72**, 1484–1503.

Vercauteren, N. and Klein, R. (2015) A clustering method to characterize intermittent bursts of turbulence and interaction with submesomotions in the stable boundary layer. *Journal of the Atmospheric Sciences*, **72**, 1504–1517.

Vercauteren, N., Mahrt, L. and Klein, R. (2016) Investigation of interactions between scales of motion in the stable boundary layer. *Quarterly Journal of the Royal Meteorological Society*, **142**, 2424–2433.

Vickers, D. and Mahrt, L. (2003) The cospectral gap and turbulent flux calculations. *Journal of Atmospheric and Oceanic Technology*, **20**, 660–672.

— (2006) A solution for flux contamination by mesoscale motions with very weak turbulence. *Boundary-Layer Meteorology*, **118**, 431–447.

— (2007) Observations of the cross-wind velocity variance in the stable boundary layer. *Environmental Fluid Mechanics*, **7**, 55–71.

Vickers, D., Mahrt, L. and Belušić, D. (2008) Particle simulations of dispersion using observed meandering and turbulence. *Acta Geophysica*, **56**, 234–256.

Webb, E. K., Pearman, G. I. and Leuning, R. (1980) Correction of flux measurements for density effects due to heat and water vapour transfer. *Quarterly Journal of the Royal Meteorological Society*, **106**, 85–100.

Van de Wiel, B. J., Vignon, E., Baas, P., Van Hooijdonk, I. G., van der Linden, S. J., Antoon van Hooft, J., Bosveld, F. C., de Roode, S. R., Moene, A. F. and Genthon, C. (2017) Regime transitions in near-surface temperature inversions: a conceptual model. *Journal of the Atmospheric Sciences*, **74**, 1057–1073.

TABLE 1 Number of meandering and non-meandering cases in the different hours of the day. The grey rows refer to nocturnal hours.

hour	meandering	non-meandering
00	57	84
01	63	79
02	52	85
03	50	74
04	74	60
05	65	73
06	55	62
07	33	71
08	14	101
09	7	73
10	4	82
11	5	66
12	4	69
13	7	61
14	7	52
15	11	65
16	13	64
17	15	88
18	49	71
19	57	60
20	62	61
21	69	67
22	57	77
23	70	72

TABLE 2 ~~Diurnal~~ Daytime meandering period for the variables depicted in Figs. 3 and 4.

	u	v	T	Rn
T_* (s)	2900	2600	3000	2400

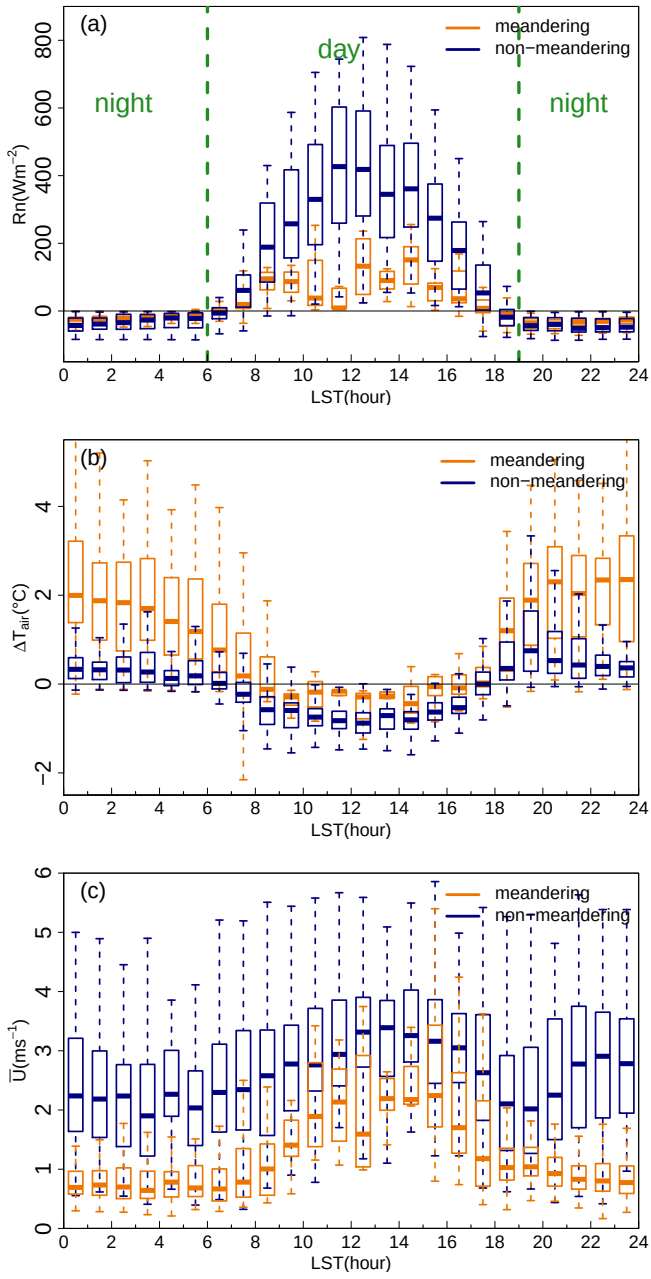

FIGURE 1 Boxplots of mean net Radiation (a), vertical air temperature difference (ΔT_{air}) between 30 and 3 m (b) and mean wind speed at 3 m (c) as a function of the time of day, for "meandering" and "non-meandering" cases.

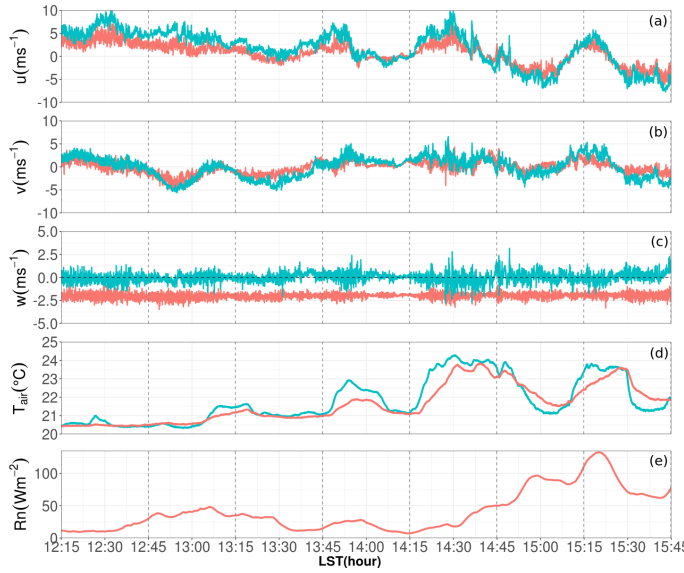

FIGURE 2 Time series of longitudinal (a), lateral (b), vertical wind velocity components (c), air temperature (d) and net radiation (e) measured at 30 (blue) and 3 m (red) on 21 December 2015. For the sake of clarity, the vertical wind velocity component at 3 m was artificially shifted (-2 m s^{-1}) in the plot.

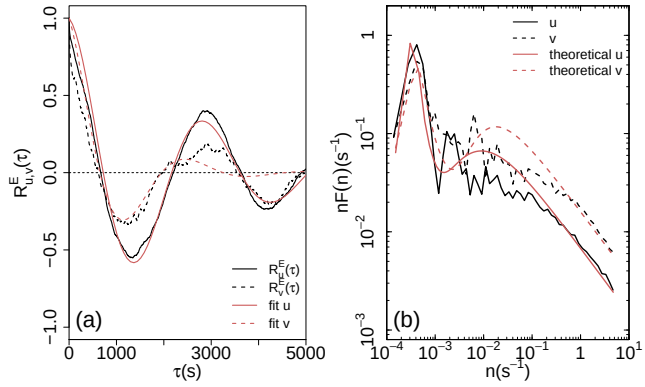

FIGURE 3 EAFs (a) and spectra (b) relative to the longitudinal (continuous line) and lateral (dashed line) wind-velocity components measured between 1400 and 1600 of 21 December 2015 at 3 m. Red lines represent the theoretical behaviour proposed by Anfossi et al. (2005) (Eq. 1) for meandering EAFs and Mortarini and Anfossi (2015) for meandering spectra.

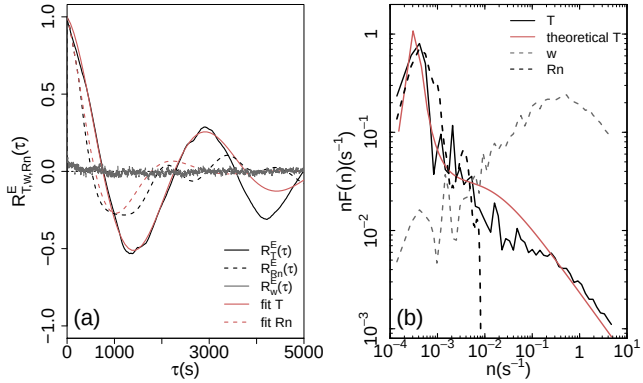

FIGURE 4 Same as Figure 3, but for sonic temperature (black continuous line), net radiation (black dashed line) and vertical velocity components (grey dashed line).

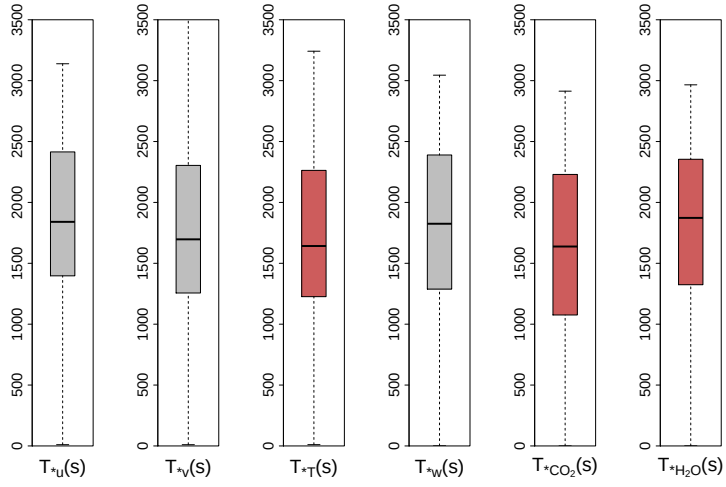

FIGURE 5 Boxplot of the nocturnal meandering time scale for the wind velocity components (grey) and scalars (red).

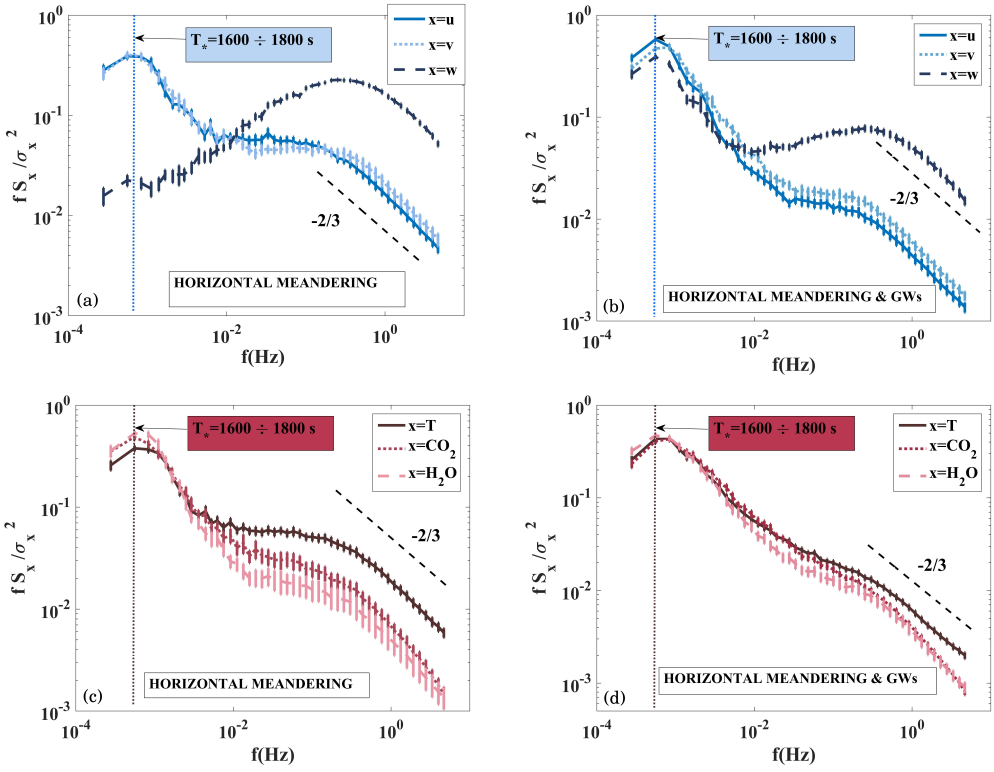

FIGURE 6 Averaged normalized spectra relative to nocturnal meandering cases for the wind velocity components (blue) and scalars (red), and in the presence (b,d) or absence (a,c) of simultaneous vertical oscillations. Vertical bars represent the standard deviation of the mean. Black dashed lines represent the -2/3 power law predicted from the Kolmogorov theory (Kolmogorov, 1941).

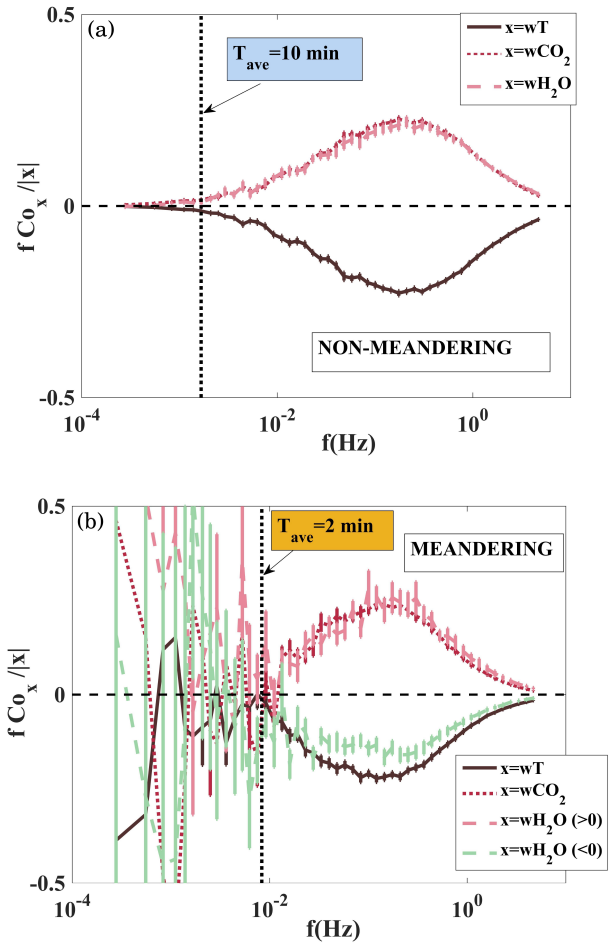

FIGURE 7 Averaged normalized co-spectra of wT, wH_2O and wCO_2, for nocturnal non-meandering (a) and meandering (b) cases. Vertical bars represent the standard deviation of the mean.

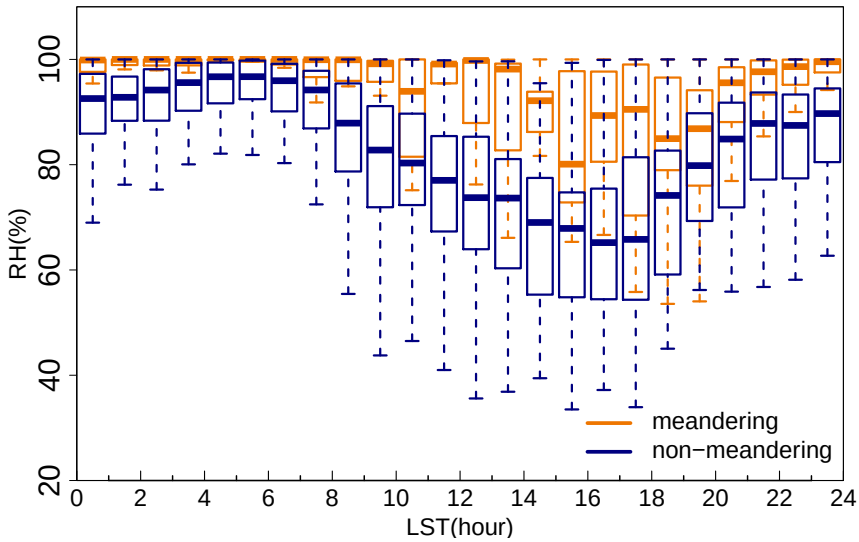

FIGURE 8 Daily evolution of the relative humidity boxplots for meandering (orange) and non-meandering (blue) cases.

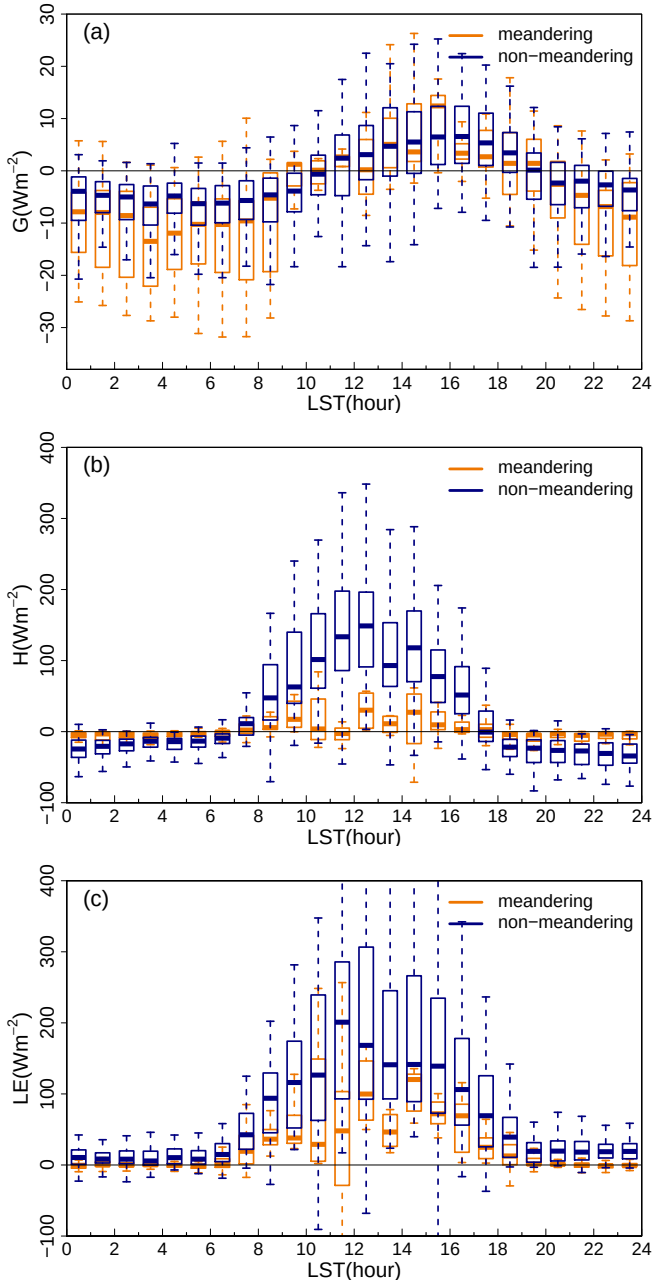

FIGURE 9 Boxplots of the diurnal cycle of: (a) soil heat flux (G), (b) sensible heat flux (H) and (c) latent heat flux (LE).

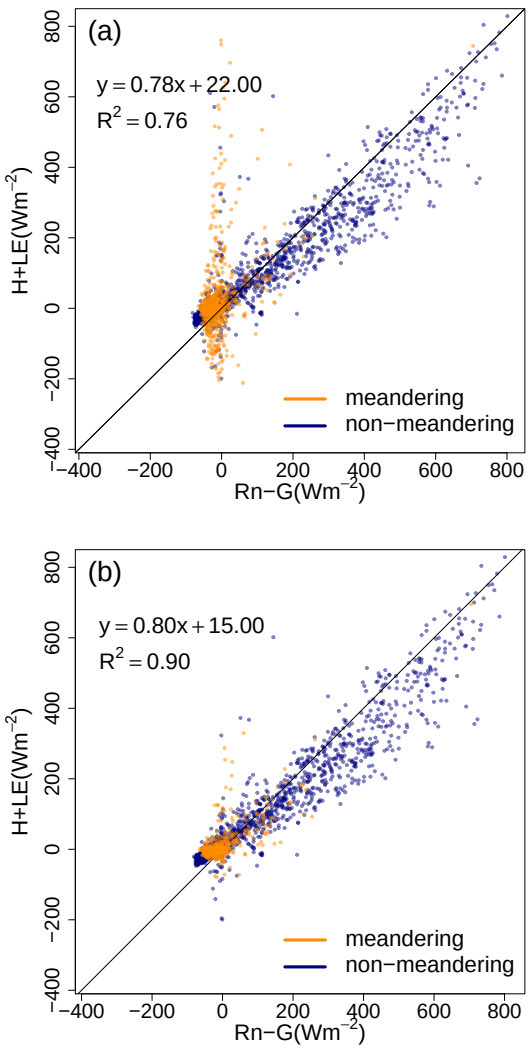

FIGURE 10 Scatterplots of the turbulent heat fluxes ($H + LE$) against the available energy ($Rn - G$). The blue (orange) points refer to non-meandering (meandering) conditions. In panel (a) the turbulent fluxes were evaluated averaging over 1 hour. In panel (b) nighttime data were evaluated using an averaging window of 2 minutes (daytime data: 15 minutes) for meandering cases and a 10 minutes (daytime data: 1 hour) window for non-meandering cases. The solid black line represents the perfect balance between the turbulent heat fluxes and the available energy.

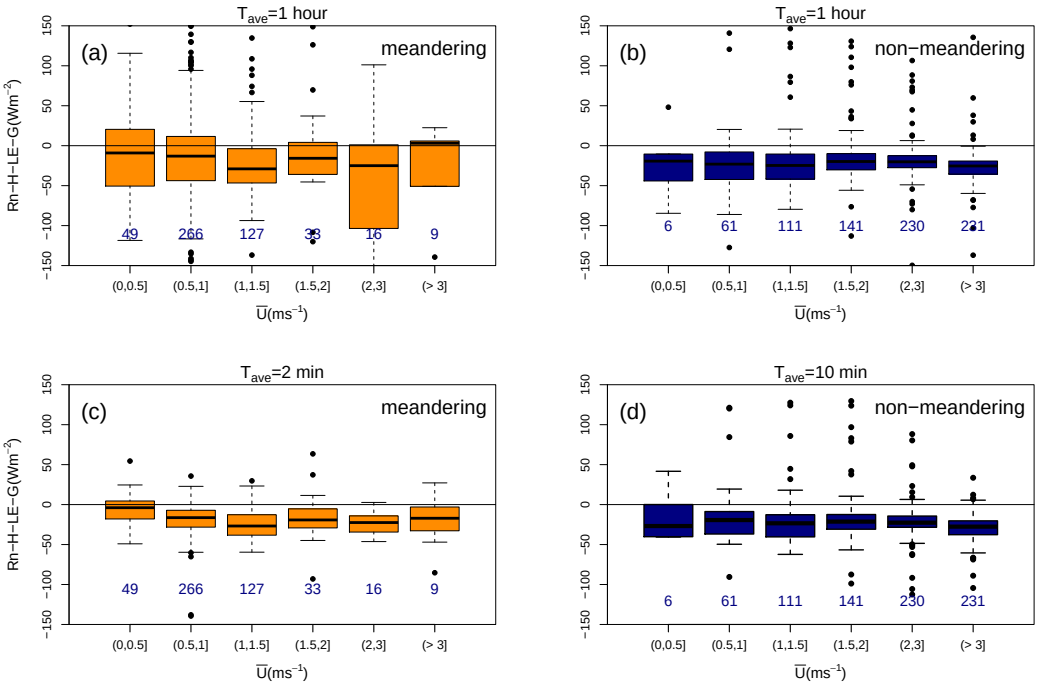

FIGURE 11 Nocturnal variation of the residual energy ($Rn-(H+LE+G)$) as a function of the mean wind speed for meandering (orange) and non-meandering (blue) data. In panels (a) and (b) the turbulent fluxes were evaluated over one hour and in panels (c) and (d) using the average period identified by the co-spectral analysis (section 4.2). Below each boxplot the number of cases used is shown.

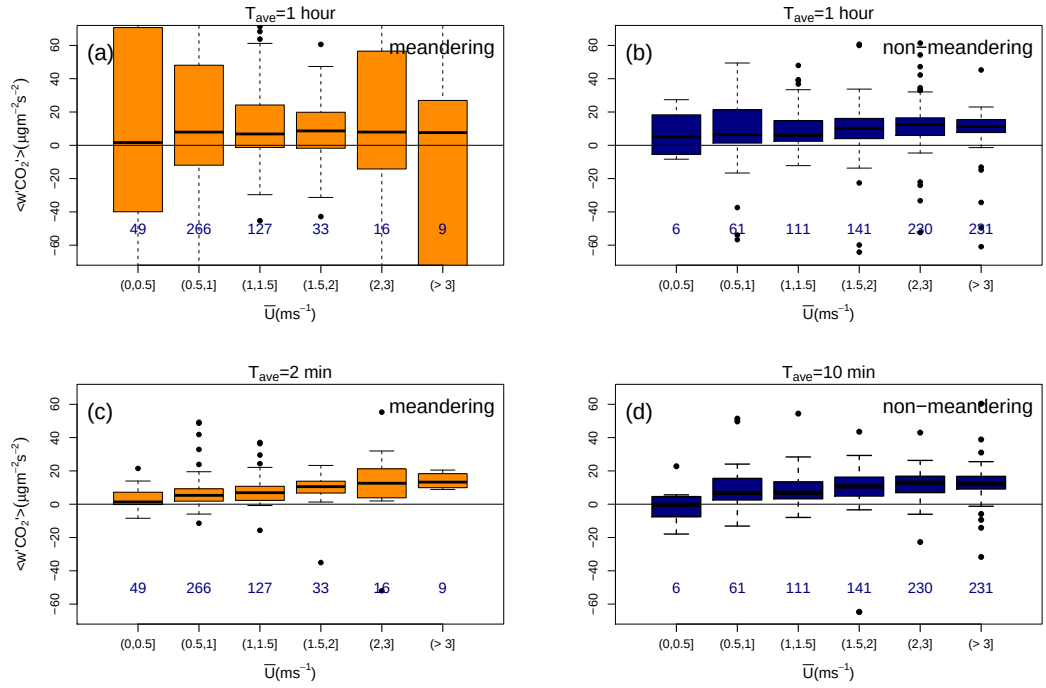

FIGURE 12 Nocturnal CO_2 vertical fluxes for meandering (orange) and non-meandering (blue) cases. In panels (a) and (b) turbulent fluxes were averaging over one hour and in panels (c) and (d) using the average period identified by the co-spectral analysis (section 4.2). Below each boxplot the number of cases used is shown.

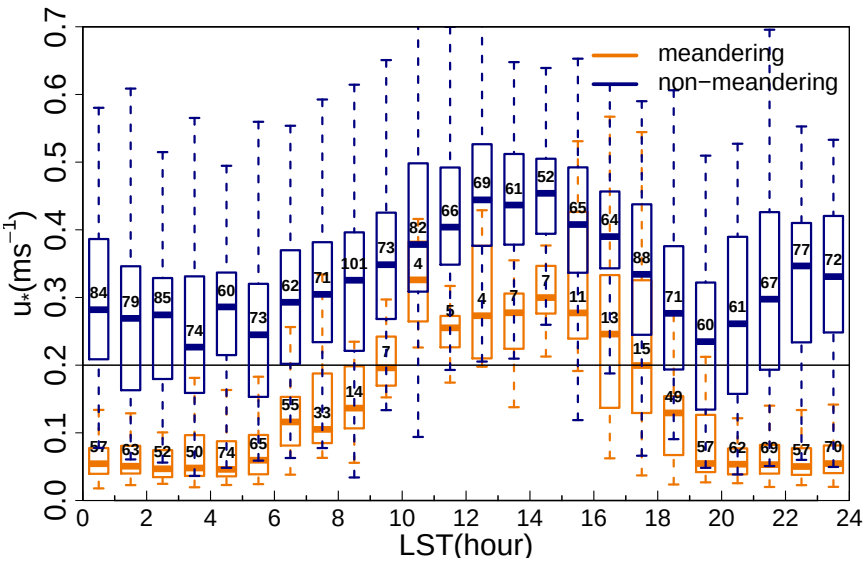

FIGURE 13 Daily evolution of the friction velocity (u_*) boxplots for meandering (orange) and non-meandering (blue) hours. Below each boxplot the number of cases used is shown.